Available online at www.sciencedirect.com
SCIENCE DIRECT®
European Journal of Mechanics B/Fluids 24 (2005) 621–641

Experimental investigation of 3D acoustic receptivity of an airfoil boundary layer due to surface vibrations

A.V. Ivanov [b], W. Würz [a,*], S. Herr [a], S. Wagner [a], Y.S. Kachanov [b]

[a] *Institut für Aerodynamik und Gasdynamik, Universität Stuttgart, Stuttgart, Germany*
[b] *Institute of Theoretical and Applied Mechanics, Russian Academy of Sciences, Novosibirsk, Russia*

Received 22 June 2004; accepted 30 December 2004

Available online 4 March 2005

Abstract

The three-dimensional acoustic receptivity of laminar boundary layers in presence of microscopic surface vibrations (the vibro-acoustic receptivity) is examined. The flow under investigation is the boundary layer on an airfoil at relatively high Reynolds numbers close to realistic ones for gliders. This flow has favourable and adverse pressure gradients and develops on a curved wall. The goal of the present study is to obtain quantitative information about the receptivity characteristics of this flow for excitation of the 3D Tollmien–Schlichting (TS) waves in cases when the frequencies of surface vibrations (f_v) have the same order of magnitudes as those of the acoustic waves (f_{ac}). The experiments were performed at controlled disturbance conditions. The 2D acoustic field was produced by loudspeakers, while the localised non-stationary surface non-uniformities were simulated by a controlled circular surface vibrator. The TS-wave generation was investigated for several values of the parameter of non-stationarity of the surface non-uniformity $K = f_v/f_{ac}$.

The receptivity was investigated in two general cases: in '*plus-regimes*' when the TS-waves were excited at combination frequencies $f_{TS+} = f_{ac} + f_v$ and in '*minus-regimes*' when the excitation occurred at frequencies $f_{TS-} = f_{ac} - f_v$. The complex (amplitude and phase) receptivity coefficients are obtained experimentally as functions of the spanwise wavenumber (and the wave propagation angle) for three different frequency ratios K and also for several TS-wave frequencies at fixed values of K. The obtained vibro-acoustic receptivity coefficients are compared with the acoustic-roughness receptivity coefficients (i.e. for $K = 0$) found in previous experiments and DNS.

Keywords: Airfoil; Boundary layer; Acoustic wave; Surface vibration; Instability wave; Receptivity coefficient

1. Introduction

The boundary-layer receptivity problem considers various mechanisms of transformation of external (with respect to the boundary-layer flow) perturbations into the eigen disturbances of the boundary layer [1]. During past years both experimental and theoretical aspects of this problem have been investigated extensively (see for review Kachanov et al. [2] and Kachanov [3]). Along with a great fundamental importance of this problem there is a significant practical motivation for its investigation connected with appearance of advanced transition prediction methods, which take into account the receptivity mechanisms. In

* Corresponding author.
E-mail address: wuerz@iag.uni-stuttgart.de (W. Würz).

0997-7546/$ – see front matter
doi:10.1016/j.euromechflu.2004.12.004

many practical situations the free-stream turbulence, the surface vibrations, and the acoustic waves represent the most important sources of the instability waves in boundary layers.

The mechanisms of generation of *two-dimensional* TS-waves by means of *unsteady surface non-uniformities* were studied (in the flat-plate boundary layer) theoretically by Gaster [4], Terent'ev [5], and Tumin and Fyodorov [6,7] and experimentally by Gilyov and Kozlov [8]. The results obtained in experiments by Gilyov and Kozlov [8] were found to be in a good agreement with calculations by Terent'ev [9] and Fyodorov [10] who studied theoretically the excitation of instability waves by means of different surface perturbations periodical in time, in particular: surface vibration, blowing-suction, and heating.

The problem of the *three-dimensional vibration receptivity* has been also studied in detail. In particular, it was shown experimentally and theoretically by Fyodorov [11], Ivanov et al. [12], Gaponenko et al. [13], Bake et al. [14], and Kachanov et al. [15] that even microscopic surface vibrations (with amplitudes of several microns, for example) are able to produce rather intensive TS-waves in 2D boundary layers (with zero, adverse, and favourable pressure gradients) and in addition cross-flow instability waves in swept-wing boundary layers. It has been found that all studied 2D boundary layers are more receptive to 3D (inclined) vibrational waves compared to the 2D ones.

The mechanisms of generation of the instability waves in 2D boundary layers by means of *acoustic perturbations in presence of steady surface non-uniformities* (roughness elements) have been studied in detail for *2D disturbances*. A great number of theoretical papers in this field are discussed by Zhigulyov and Tumin [16], Goldstein and Hultgren [17], Kerschen [18], Kozlov and Ryzhov [19], Morkovin and Reshotko [20], Choudhari and Streett [21], Crouch [22], Choudhari [23], and others. In particular an excitation of the 2D instability waves by acoustics on 2D roughness elements was studied *experimentally* by Aizin and Polyakov [24], Kosorygin et al. [25], Kosorygin [26], Saric et al. [27], Wiegel and Wlezien [28], Kosorygin et al. [29], and others. It was found that the acoustics excites the 2D TS-waves rather effectively even on microscopically small non-uniformities. The receptivity coefficients were estimated in these studies for different acoustic frequencies, roughness shapes, and acoustic-wave inclination angles. A good agreement between theory and experiment was usually observed.

At the same time, the problem of the *three-dimensional* acoustic-roughness receptivity is studied considerably weaker, especially experimentally. Choudhari and Kerschen [30] probably were the first who obtained theoretical results on generation of TS-waves by acoustics on a three-dimensional surface roughness element (or localised three-dimensional suction) for a two-dimensional boundary layer. A similar problem was investigated theoretically by Tadjfar and Bodonyi [31] with the help of non-stationary linearised three-dimensional equations for the asymptotic triple-deck model of the two-dimensional boundary layer. A qualitative comparison of these results with experiments by Gilyov and Kozlov [8] and Tadjfar [32] was also performed in this paper. The excitation of TS-waves by acoustics on three-dimensional roughness elements, such as an oblique surface roughness strip and a circular roughness, was investigated experimentally by Zhou et al. [33]. Choudhari and Kerschen [30] found these results to be in a good qualitative agreement with theory. Cullen and Horton [34] studied experimentally the acoustic receptivity for a stationary localised three-dimensional roughness in a two-dimensional boundary layer, but no quantitative receptivity coefficients were obtained in this work.

It has been also found that the acoustic fields can represent a possible source for the cross-flow instability waves in swept-wing boundary layers. As shown by Crouch in [35] and [22], the acoustic receptivity mechanism does exist and can play a certain role in the transition process at high enough levels of acoustic excitation. In these theoretical works a scattering of the acoustic wave on a stationary localised surface non-uniformity (roughness) was investigated. This mechanism was observed and investigated experimentally by Ivanov et al. [36,37] on a model of a swept wing. The same authors have studied in [38] the case of an unsteady surface non-uniformity, i.e. when it is represented by a localised surface vibrator (oscillated with a low frequency). In this case, the mechanism of excitation of the cross-flow instability wave was quasi-stationary. The values of the acoustic receptivity coefficients were estimated in these experiments. In a qualitative agreement with theory the acoustic receptivity due to surface non-uniformities was found to be rather weak in 3D boundary layers compared to the 2D ones.

In 2D boundary layers the 3D acoustic-roughness receptivity coefficients were obtained for the first time experimentally by Würz et al. [39] for a single acoustic frequency and compared with calculations in Würz et al. [40]. More detailed experimental and numerical results were presented for several disturbance frequencies by the same authors in [41]. It was found that the 3D acoustic-roughness receptivity of the 2D boundary layer is significantly stronger compared to the 2D case. The receptivity coefficients obtained in accompanied DNS were found to be in a very good agreement with the experimental ones.

The *acoustic receptivity* in presence of *essentially non-stationary surface non-uniformities*, i.e. the surface vibrations, has not been studied yet experimentally in cases when the vibrational (f_v) and acoustical (f_{ac}) frequencies are comparable with each other and when the parameter of non-stationarity of the surface non-uniformity $K = f_v/f_{ac}$ is essentially non-zero one. Meanwhile, this receptivity mechanism seems to be very important in some cases because, in particular, it can provide a redistribution of the disturbance energy in the frequency-wavenumber spectrum. For example, the boundary layer might be stable to the TS-waves excited by the surface vibrations themselves (at frequency f_v) and to those excited by the acoustic waves on surface roughness (at acoustic frequency f_{ac}), while the TS-waves, excited by the vibro-acoustic receptivity at combination frequencies $f_{TS} = f_{ac} \pm f_v$, can be amplified and lead to transition.

The goal of the present study was to close this gap and to investigate the three-dimensional problem of scattering of acoustic waves on surface vibrations, localised in the streamwise and spanwise directions, for the case when parameter K is between zero and one and the boundary layer is unstable to the TS-waves excited at combination frequencies.

2. Experimental procedure

2.1. Experimental model and base flow characteristics

A sketch of the experimental setup is presented in Fig. 1. The experiments were carried out in the Laminar Wind Tunnel (LWT) of the IAG. The LWT is an open return tunnel with a turbulence level less than 2×10^{-4}. The boundary layer measurements were performed on a symmetrical airfoil section 'XIS40MOD' (Würz [42]) with 15% thickness (installed at zero angle of attack) at a Reynolds number of 1.23×10^6 based on the arclength $s_{\max} = 0.615$ m measured from the leading edge. The airfoil was manufactured from reinforced fibreglas in a numerically controlled milled mould. Remaining roughness r.m.s. heights of the model surface are in the order of 0.5 μm measured with a precision surface measuring system. The controllable element modeling the surface vibration (hereafter the vibrator) was mounted at the streamwise coordinate $s = s_v = 123$ mm ($s_v/s_{\max} = 0.2$). The free stream velocity at this position (measured at the boundary-layer edge) was $U_{ev} = 36$ m/s, the Reynolds number $Re = U_{ev}\delta_{1v}/\nu$ based on this velocity and the boundary displacement thickness at the position of the vibrator ($\delta_{1v} = 0.356$ mm) was 850 (ν is the air kinematic viscosity). The airfoil, the base flow (including the Reynolds number), and the values of the frequency parameter $F = 2\pi f \nu / U_{ev}^2$ of the instability waves under investigation were similar to those studied by Würz et al. [41], in order to provide the comparability of the receptivity characteristics in the two experiments.

The boundary layer measurements were performed with a computer controlled traversing system, which allows scans in wall-normal direction y with an accuracy of 5 μm and scans in spanwise direction z with an accuracy of 0.1 mm. In addition to the hot-wire support a small static pressure probe was fixed on this system which was used during measurements as a velocity reference at the boundary layer edge.

The basic pressure distribution was evaluated from the readings of 48 pressure taps, with the boundary layer traversing mechanism placed at the decided measurement position to take its influence into account. The measured values were compared with distributions calculated from XFOIL (see e.g. Drela and Giles [43]) for a series of slightly different angles of attack until they gave the best fit to the experimental data. This distribution (Fig. 2) was then used for the calculation of boundary layer profiles with a finite difference scheme according to Cebeci and Smith [44]. Finally, the stability characteristics were calculated with a shooting solver (Conte [45]) for the solution of the Orr–Sommerfeld equation.

Due to the long instability ramp of the airfoil the shape factor $H_{12} = \delta_1/\delta_2$ increases nearly linearly from the value $H_{12} = 2.58$ at $s_v/s_{\max} = 0.2$ to $H_{12} = 2.71$ at the end of the measurement region at $s/s_{\max} = 0.33$ (δ_2 is the boundary layer momentum thickness).

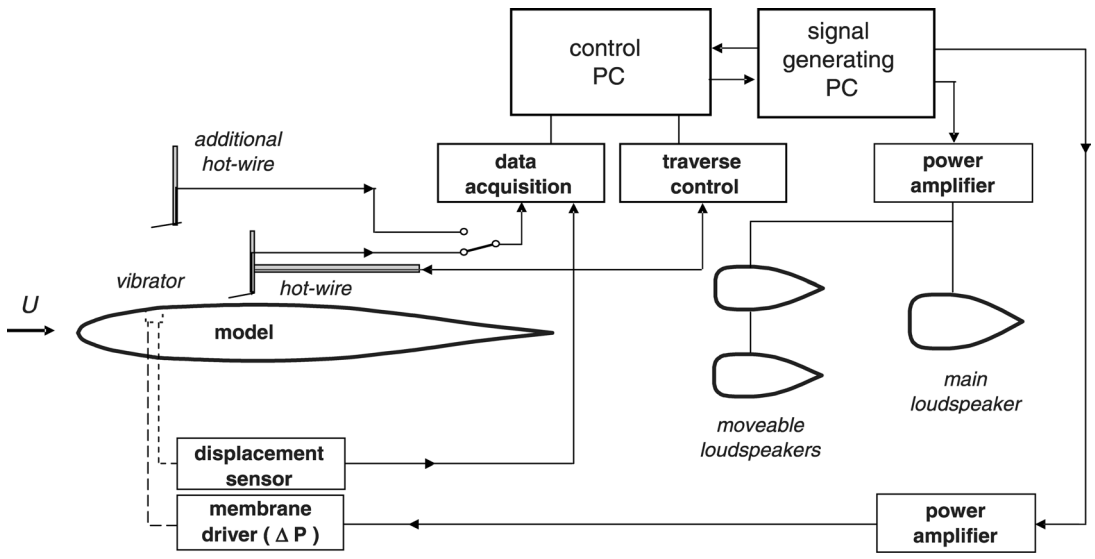

Fig. 1. Sketch of the experimental setup.

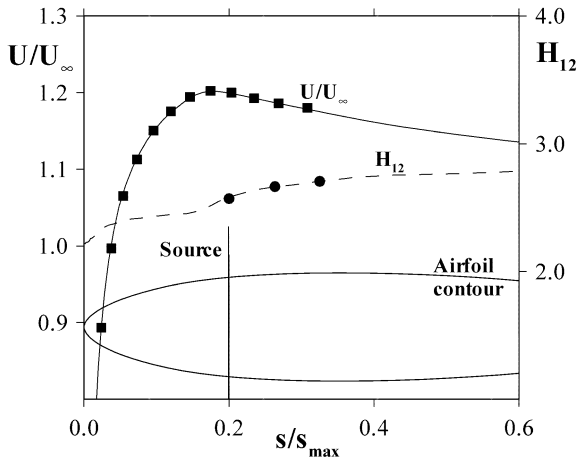

Fig. 2. Calculated velocity distribution and development of the shape factor H_{12} together with the airfoil contour and the position of the surface vibrator. Symbols denote measured values.

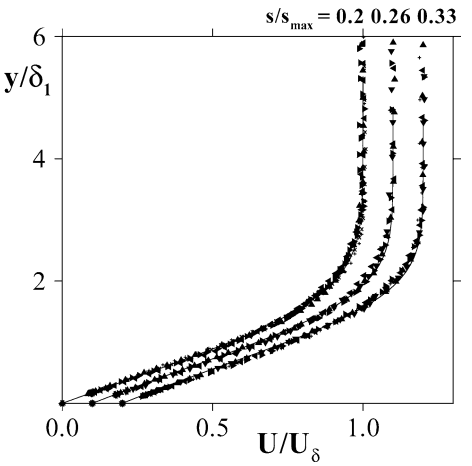

Fig. 3. Mean velocity profiles for different streamwise positions. Profiles shifted by $\Delta(U/U_\delta) = 0.1$. Lines denote boundary layer calculations.

Mean flow velocity profiles measured at three downstream positions are presented in Fig. 3 (symbols) together with the calculated ones (lines), which fit quite well to the experimental data. The shape factor $H_{12} = 2.58$ measured at the position of the vibrator ($s_v/s_{max} = 0.2$) is very close to the Blasius value of $H_{12} = 2.59$. Nevertheless, due to prehistory effects of the boundary layer the shape of the profile can show in detail some deviations from the Blasius profile. Despite this fact, stability calculations for the present configuration showed that these deviations are negligible.

2.2. Controlled disturbances

The acoustic waves were generated by a set of loudspeakers placed on the centerline of the wind tunnel, downstream the test section (Fig. 1). This was locally a quasi-2D acoustic field consisted of a mixture of direct waves propagating upstream and a certain amount of reflected waves propagating downstream. Special measurements (with a slanted hot wire) have shown that, the angle of inclination of the velocity fluctuation vector of the acoustic wave (in the (x, z)-plane) with respect to the mean flow direction is very small, typically below 10°.

Since the acoustic wavelength depends on the air temperature, any variation of the latter changes the structure of the acoustic field in the wind-tunnel and, consequently, the acoustic amplitude and phase over the surface vibrator. This circumstance forced us to check the constancy of the acoustic parameters during the main receptivity measurements. In experiments by Würz et al. [41] this was done periodically by means of positioning the hot-wire probe over the vibrator after every spanwise scan. In this experiments an additional (second) hot-wire probe was used for such measurements. The hot-wire was mounted on a thin moveable rod, which played a role of a simple traverse (see Fig. 1).

In order to obtain a desirable intensity of acoustic-field at different air-temperature conditions and frequencies of acoustic, two additional, moveable loudspeakers were used (Fig. 1). Their streamwise position was adjusted in a way to provide the necessary amplitude of the acoustic wave at the vibrator position.

A sketch of the surface vibrator used in the present experiment is shown in Fig. 4. The vibrator had parameters similar to those in experiments by Würz et al. [41]. Its plastic circular membrane (1) had diameter of 6 mm and was driven by pressure fluctuations produced by the membrane driver based on a powerful loudspeaker. This loudspeaker was mounted in an airtight housing and pressure balanced by a connection to a static pressure orifice at the same streamwise position as the membrane to avoid steady deflection. The membrane was installed precisely flush with the model surface (2) and sealed (4). In order to provide a control of membrane oscillations a fiber-optic displacement sensor 'Philtec D12' was used to measure the amplitude in the membrane center. This sensor has a linear response up to 20 kHz with a resolution of 0.56 μm in a 0.5 mm measurement range. Thus, the complete information about the membrane oscillations was permanently available during the measurements (see also data the acquisition procedure in Section 2.3).

The spatial shape of the membrane oscillations was measured before mounting the vibrator into the model and additionally after the experiments with the help of a laser triangulation vibrometer 'Micro-Epsilon LD1605-0.5' (linearity ±0.2% for a range of ±0.25 mm). A typical spatial distribution of the oscillation amplitudes over the vibrator surface normalised by the amplitude in the membrane center is presented in Fig. 5. This shape of the membrane oscillation turned out to be practically independent of both the frequency and the amplitude of excitation. The phase of the oscillations were found to be constant over the whole

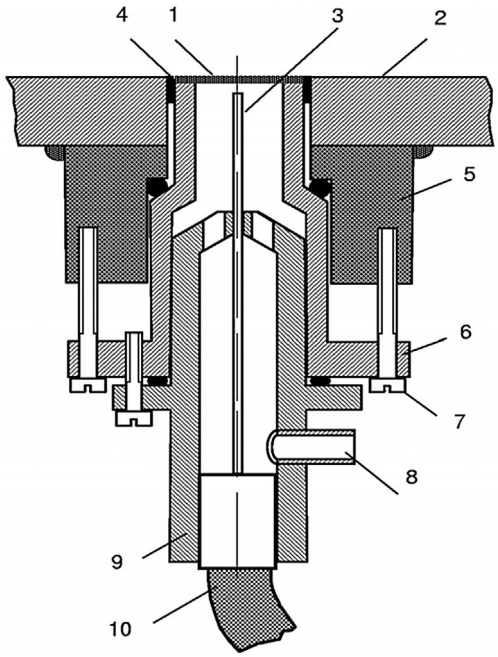

Fig. 4. Sketch of the surface vibrator. 1 – membrane, 2 – model surface, 3 – displacement sensor tip, 4 – sealant, 5 – mounting, 6 – casing, 7 – adjustment screws, 8 – pneumatic pipe connector, 9 – mounting for fiber cable and pneumatic pipe, 10 – fiber cable.

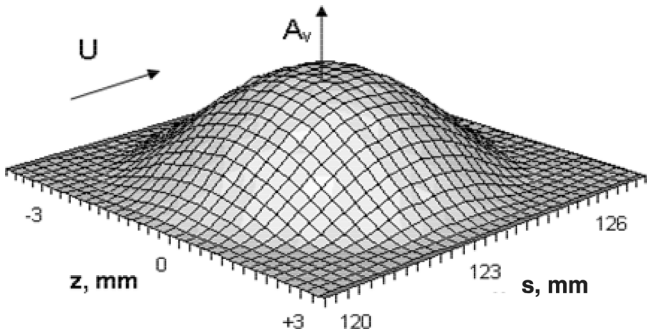

Fig. 5. Typical distribution of normalised amplitudes of vibrations over the membrane surface.

membrane surface, therefore the instantaneous shape of the membrane deflection remains the same at every time instant and corresponds to that shown in Fig. 5.

2.3. Procedure of measurements and data acquisition

To find experimentally the receptivity coefficients it was necessary to determine the initial (i.e. at the position of the vibrator) amplitudes of the excited TS-waves. They cannot be measured directly due to the presence of various other perturbations in the vibrator-near-field, such as continuous-spectrum instability modes and forced (bounded) fluctuations. Therefore, the hot-wire measurements in the boundary layer were performed far enough downstream the vibrator, where only eigen boundary-layer oscillations (i.e. the TS-waves) dominated. In the present experiments normally 4 to 5 spanwise scans (with 40 to 60 spatial points in each) were measured downstream the vibrator in every studied regime of excitation. These measurements provide the information about spatial development of the excited wave-trains. In every spanwise scan the hot-wire probe was positioned at a fixed distance from the wall $y/\delta_2 = 2.2$, which corresponded approximately to the TS-wave amplitude maximum in y-profiles (see [41] for more detail). This position was adjusted during every spanwise scan by keeping U/U_e constant at a corresponding value.

The system of signal excitation and data acquisition is also presented in Fig. 1. For the hot-wire measurements the modified DISA 55P15 boundary layer probe with 1 mm wire in length was used together with a DISA 55M10 bridge. The second, additional hot-wire (with an additional DISA 55M10 bridge) was used for acoustic measurements. The calibration of the hot-wires was made according to Kings law and the coefficients were optimised for minimum standard deviation. During run time the reading from the static probe at the traversing system was used to adjust the absolute values of the velocities calculated from the hot-wire data. The DC-outputs of the hot-wire anemometers were low-pass filtered. The AC-output was high-pass filtered with a first order low-noise filter with a cut-off frequency of 100 Hz. A programmable amplifier was used to fit the signal always optimally to the input range of a 12-bit A/D-converter. Prior to sampling, the signal was low-pass filtered in addition (4th order) at 4400 Hz to omit aliasing problems connected with the sampling frequency. Two PCs were used simultaneously. The first one was used for the data acquisition, the traversing mechanism control, and the sequencing. The second one was used for the signals generation. The vibrational and acoustical frequencies, as well as the digital sampling trigger, were generated by a D/A-converter of this PC. The acoustic, vibrational, and combination frequencies had integer number of periods in one sampling,

Table 1
Studied regimes of disturbance excitation

Type of regime	Name of regime	Parameter $K = f_v/f_{ac}$	Acoustic frequency f_{ac} [Hz]	Vibration frequency f_v [Hz]	TS-wave frequency f_{TS} [Hz]
Plus-regimes	$K = 0.217\, f_{TS2+}$	0.217	873	190	1063
$f_{TS+} = f_{ac} + f_v$	$K = 0.217\, f_{TS3+}$	0.217	1309	285	1594
	$K = 0.217\, f_{TS4+}$	0.217	1359	295	1654
	$K = 0.434\, f_{TS2+}$	0.434	742	323	1065
	$K = 0.980\, f_{TS2+}$	0.980	537	526	1063
Minus-regimes	$K = 0.217\, f_{TS2-}$	0.217	1359	295	1064
$f_{TS-} = f_{ac} - f_v$	$K = 0.217\, f_{TS3-}$	0.217	2038	443	1595
	$K = 0.434\, f_{TS2-}$	0.434	1886	820	1066

and all frequencies were strictly phase locked because they were produced by a single quartz-based clock. This provided the possibility to represent each of these signals by a single Fourier-series coefficient after the FFT and enabled the online control of the whole frequency spectrum.

The data acquisition was started with a fixed phase relationship to the vibrator signal, which played a role of a reference signal. After a prescribed number of generated signal periods (needed for establishment of the acoustic field and the TS-wave train) five realisations, consisted of 4096 points each, were collected and ensemble averaged in the time domain. The FFT analysis was performed and frequency spectra of boundary layer perturbations were monitored online. These data contained the information on amplitudes and phases of disturbances developing in the boundary layer in a wide frequency range.

Exactly in the same way, the output of the displacement sensor Philtec D12 was recorded in each point of measurements. This signal contained the information about the membrane oscillation amplitudes. The acoustic intensity measurements were performed immediately before and after every spanwise scan. During these measurements the second hot-wire was switched on in the measurement circuit instead of the main hot-wire and moved into the vibrator position for the acoustic measurements (3 to 6 samples). Additionally, in every set of measurements two or three normal-to-wall profiles were taken, including the profile over the vibrator center ($s_v = 123$ mm, $z = 0$).

2.4. Studied range of disturbance parameters

Three different values of the parameter of non-stationarity of the surface non-uniformity $K = f_v/f_{ac}$ were investigated: $K = 5/23 \approx 0.217$, $K = 10/23 \approx 0.434$, and $K = 98/100 = 0.98$. As was mentioned above, the generation of TS-waves occurs at combination frequencies $f_{TS+} = f_{ac} + f_v$ (*plus-mode*) and $f_{TS-} = f_{ac} - f_v$ (*minus-mode*). During selection of the specific values of the acoustic and vibration frequencies the following factors were taken into account: (i) all main frequencies (f_{TS}, f_{ac}, f_v) must have an integer number of periods in the experimentally recording signal realisation and correspond to the Fourier-series coefficients, (ii) one of frequencies f_{TS} of the generated instability waves (either f_{TS+} or f_{TS-}) must lie in the region of the amplified TS-wave frequencies and to be close to one of frequencies investigated by Würz et al. [41], and (iii) the frequencies of the excited TS-waves should not overlap with the frequencies associated with any other signals of different physical nature. For example, the value of parameter $K = 1.0$ is difficult to investigate experimentally, because in this case second harmonics of the vibration and acoustic frequencies ($2f_v$ and $2f_{ac}$) overlap with the TS-wave combination frequency $f_{TS+} = f_{ac} + f_v$.

The chosen regimes of the acoustic-vibration interaction are listed in Table 1. Set of regimes: $K = 0.217\, f_{TS2+}$, $K = 0.434\, f_{TS2+}$, and $K = 0.98\, f_{TS2+}$ (as well as $K = 0.217\, f_{TS2-}$ and $K = 0.434\, f_{TS2-}$) was measured in order to obtain comparable data on the vibro-acoustic receptivity, when the same (approximately) TS-wave frequency is generated by different frequency-combinations of vibrations and acoustics. Meanwhile, the pairs of regimes $K = 0.217\, f_{TS2+}$, $K = 0.217\, f_{TS3+}$ and $K = 0.217\, f_{TS2-}$, $K = 0.217\, f_{TS3-}$ where measured in order to investigate the influence of frequency of the excited TS-wave at a fixed value of parameter K. An additional set of data for the plus-regime, named $K = 0.217\, f_{TS4+}$, was obtained from the regime $K = 0.217\, f_{TS2-}$, when $f_{ac} = 1359$ Hz, $f_v = 295$ Hz. In this regime of measurements (in which the frequency $f_{TS2-} = f_{ac} - f_v$ was considered as the main one) the plus combination frequency $f_{TS2+} = f_{ac} + f_v = 1654$ Hz also gave reliable data, which were processed as well.

The positions of the excited TS-wave frequencies ($f_{TS2} = 1063$–1066 Hz, $f_{TS3} = 1594$–1595 Hz and $f_{TS4} = 1654$ Hz) in the stability diagram, calculated for 2D TS-modes, are shown in Fig. 6. They correspond to the frequencies investigated in [41].

A sketch of the chosen regimes is presented graphically in Fig. 7, where the TS-wave frequencies excited in various studied regimes are indicated in the plane (f_{TS}, K) together with the regimes studied in experiments and DNS in [41]. According

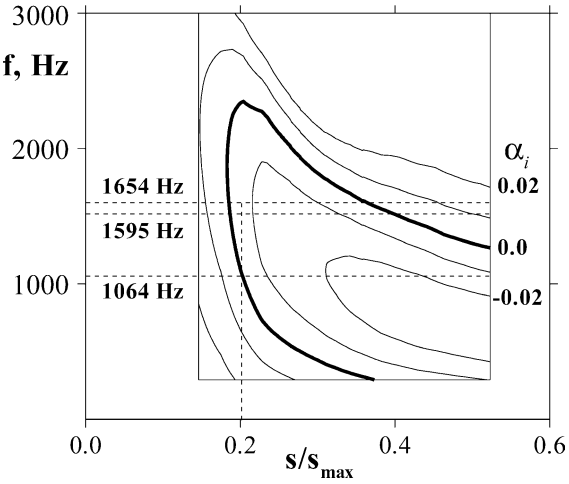

Fig. 6. Studied ranges of parameters depicted in the stability diagram for 2D TS-waves. Surface vibrator position is $s/s_{\max} = 0.2$.

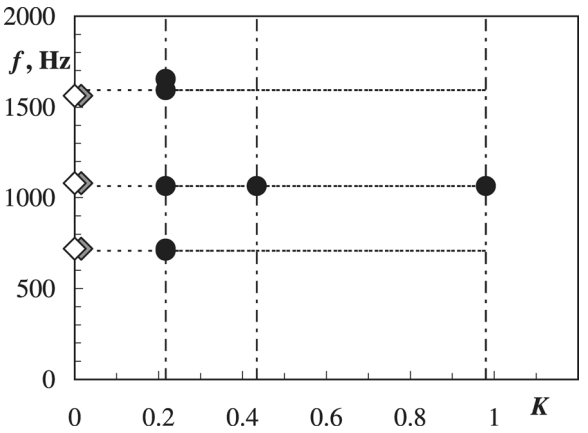

Fig. 7. Sketch of investigated regimes in the plane: TS-wave frequency f vs. the parameter of non-stationarity of surface non-uniformity K. Circles: present experiments, closed rhombs: experiments [41], open rhombs: DNS [41].

to Table 1, every TS-frequency is supposed to be generated twice: in a plus-regime and in a minus-regime. (The case of $K = 0.98$ represents an exception since the TS-waves excitation at minus-regime is hardly realisable in this case.) Thus, the chosen regimes of experiments capture a considerable region of values of the excited TS-waves frequencies and parameters of non-stationarity K, as well as frequencies of the involved surface vibrations and acoustic waves (Fig. 7 and Table 1).

Some additional measurements were performed to check the linearity of the receptivity problem under investigation. For this, some of spanwise distributions were measured several times, when the vibration and acoustic amplitudes were varied. The measured amplitude distributions have been compared with each other after their normalisation by a product of the acoustic wave amplitude and the amplitude of the surface vibration (see Section 6.2).

Note that in view of some peculiarities found for the minus-regimes, the results of measurements for these cases will be presented separately (Section 6.3).

3. Boundary-layer perturbations observed in plus-regimes

A typical frequency spectrum of the hot-wire signal, measured in the boundary layer downstream the surface vibrator ($s =$ 150 mm) in presence of acoustics, is shown in Fig. 8 in logarithmic scale. The spectrum is obtained in regime $K = 0.217 f_{\mathrm{TS2+}}$. The vibration frequency here is $f_{\mathrm{v}} = 190$ Hz (marked with a circle), while the acoustic frequency is $f_{\mathrm{ac}} = 873$ Hz (marked with a closed triangle). The perturbations at these frequencies, as expected, have the highest amplitudes in the hot-wire signal.

It is seen that the surface vibrations do generate the instability waves very effectively in a qualitative agreement with the results obtained in previous investigations of the vibrational receptivity [12–15]. In the present case, the localised surface vibration with amplitude of 37 μm in the vibrator center (i.e. about 1% of the boundary-layer displacement thickness $\delta_{1\mathrm{v}}$) provides the excitation of the boundary-layer velocity fluctuations at frequency $f_{\mathrm{v}} = 190$ Hz with the amplitude of about 0.1% (and up to 0.5% further downstream). Most of other spectral modes, having noticeable amplitudes in the spectrum in Fig. 8, correspond to frequencies of the second, third, and other higher harmonics of the main vibrational frequency. It has been found that the membrane oscillates at these frequencies as well (with amplitudes in the order of 1 μm and less), therefore these higher harmonics are also excited by the surface vibrations.

The signal at the acoustic frequency is also very intensive. It consists mainly of a mixture of signals associated with: (i) the acoustic field itself, including the Stokes layer in the near-wall region, (ii) the vibrations of the hot-wire probe and the model surface, and (iii) the TS-waves generated by the acoustics on steady non-uniformities of the base flow and the airfoil. In this case, the amplitude of the velocity fluctuations associated with the acoustic wave, measured in the free stream above the vibrator, was about $u'_{\mathrm{ac}} = 0.020\%$ (in other regimes of measurements it was typically between 0.017 and 0.028%).

The modes produced by the interaction of the acoustic field with the surface vibrations (due to the vibro-acoustic receptivity mechanism) are observed at combination frequencies; here: $f_{\mathrm{TS-}} = f_{\mathrm{ac}} - f_{\mathrm{v}} = 683$ Hz (*minus-mode*); and $f_{\mathrm{TS2+}} = f_{\mathrm{ac}} + f_{\mathrm{v}} = 1063$ Hz (*plus-mode*). These spectral modes are marked in Fig. 8 with squares. In the present streamwise position

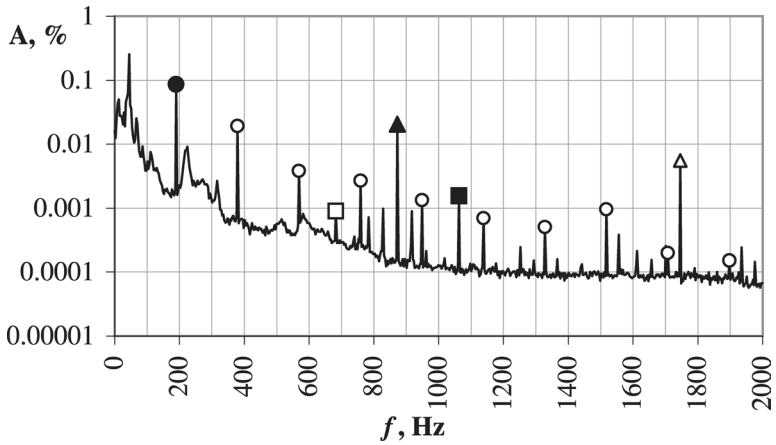

Fig. 8. Typical frequency spectrum of the hot-wire signal measured in the boundary layer in plus-regimes. Regime $K = 0.217 f_{TS2+}$, $s = 150$ mm. Closed circle: vibration frequency, open circles: harmonics of vibration frequency, closed triangle: acoustic frequency, open triangle: harmonic of acoustic frequency, closed square: plus combination mode, open square: minus combination mode.

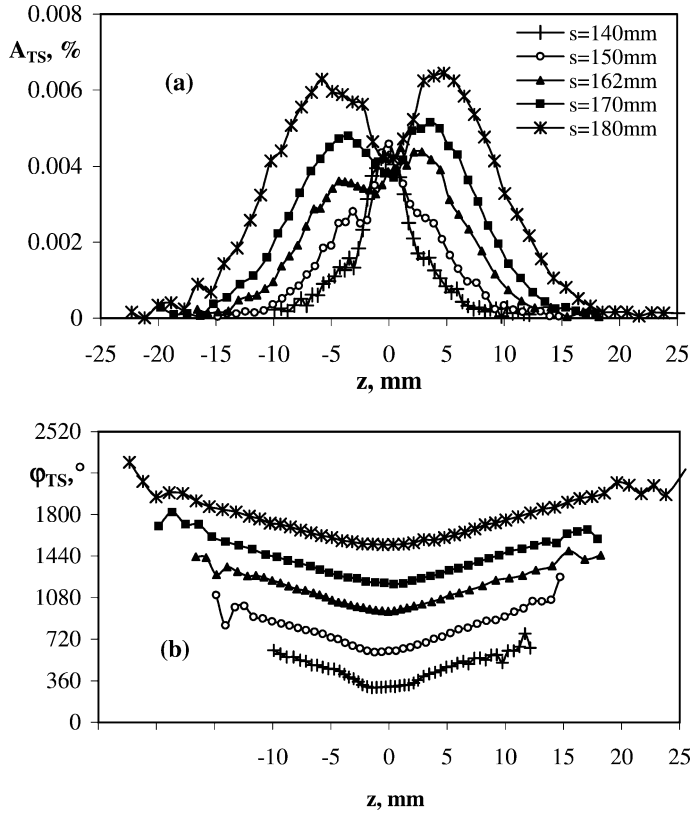

Fig. 9. Spatial development of amplitudes (a) and phases (b) of TS-waves excited at plus combination frequency $f_{TS2+} = f_{ac} + f_v = 1063$ Hz in the regime $K = 0.217 f_{TS2+}$.

(27 mm downstream the vibrator) the amplitudes of these combination waves are relatively low. Of course, the relative values of amplitudes of different spectral modes change further downstream. In the regime presented in Fig. 8 the *plus* combination mode under investigation ($f_{TS2+} = 1063$ Hz) corresponds to one of the most amplified TS-waves. The spatial development of disturbances at this frequency is presented in Fig. 9 (for the same regime $K = 0.217 f_{TS2+}$) as a set of spanwise distributions of

the TS-wave amplitude (Fig. 9(a)) and phase (Fig. 9(b)) measured at several streamwise positions. Disturbance amplitudes are presented in percentage of the local boundary-layer edge velocity. The distributions are typical for the amplifying wave-train of instability modes. In the present case these modes are *initiated by vibro-acoustic receptivity mechanism* and represent the main subject of the present study. The distributions like those presented in Fig. 9 where used for the subsequent data processing in order to obtain the complex receptivity coefficients for scattering of acoustic waves on surface vibrations. Similar data sets were obtained also for all other studied regimes indicated in Table 1.

4. Procedure of determining the receptivity function

To determine experimentally the complex vibro-acoustic receptivity functions the data were processed according to the technique, applied in [12–14] for the vibration receptivity problem and adopted in [39–41] for the acoustic-roughness receptivity case. In this section, we only enumerate briefly the main steps of the data processing procedure. These steps are the following:

1) The normalisation of the measured spanwise amplitude and phase distributions for the excited TS-waves by the amplitude and phase of the surface vibrations (in the vibrator membrane center).

2) The normalisation of the distributions obtained after the first step by the acoustic-wave amplitude and phase measured above the vibrator. As was mentioned above (see Section 2.3), direct measurements of the acoustic intensity were performed only in the beginning and in the end of every spanwise scan. However, during the subsequent data processing it turned out to be possible to reconstruct the amplitude and the phase of the acoustic wave for every point of measurements. The acoustic amplitude was determined using its empirical dependence on the air temperature. This dependence was extracted from the hot-wire measurements of the acoustic wave, performed simultaneously with the air temperature measurements. The readings of the membrane oscillations at the acoustic frequency also gave additional information about the acoustic fluctuations, mainly on its phase.

3) The preparation of the data for the spatial (in the spanwise direction) Fourier transform, namely an interpolation of the measured spanwise distributions in order to have equidistant points along the spanwise coordinate, with the same spacing as in 6).

4) The complex Fourier transform of the spanwise distributions of disturbance amplitudes and phases. An example of the resulting spanwise-wavenumber spectra is presented in Fig. 10 for regime $K = 0.217 f_{\mathrm{TS2+}}$. The TS-wave spectral amplitudes are shown in Fig. 10(a) in logarithmic scale versus the non-dimensional spanwise wavenumber normalised by the boundary-layer displacement thickness $\delta_{1\mathrm{v}}$ measured at the position of the surface vibrator. The corresponding spectral phases are presented in Fig. 10(b).

5) The reconstruction of initial amplitudes and phases of the excited TS-waves. To obtain the disturbance amplitudes at the position of the vibrator ($s_{\mathrm{v}} = 123$ mm), linear stability calculations were performed for the experimental conditions. The calculated amplification curves covered the location of the vibrator and the downstream region, where the experimental data were obtained. The theoretical curves were matched with the experimental points by means of a least square fit method. To obtain the initial phases, linear approximation of the streamwise phase distributions (measured for every fixed spanwise wavenumber) was performed and the approximated line was used for the phase extrapolation to the vibrator position. An illustration of these procedures is presented in Fig. 11 (regime $K = 0.217 f_{\mathrm{TS2+}}$) for several values of the spanwise wavenumber β (Fig. 11(a) — amplitudes, Fig. 11(b) — phases). Points in Fig. 11 correspond to the experimental values, lines in Fig. 11(a) show the calculated amplification curves matched with the experimental points, and lines in Fig. 11(b) represent the results of the approximation of phase distributions. The reconstructed initial values of the TS-wave amplitudes and phases obtained for various spanwise wavenumbers are shown Fig. 11 with crosses. The corresponding initial spanwise-wavenumber spectra are also presented in Fig. 10 ($s_{\mathrm{v}} = 123$ mm) for all studied spanwise wavenumbers. (Note that the accuracy of determination of the initial disturbance phases is expected to be rather limited due to their very fast downstream growth.)

6) In order to obtain the *surface vibration spectrum*, the membrane shape function (the amplitude part of which is shown in Fig. 5) was subjected to a spatial double Fourier transform. As a result, the 2D spectrum of surface vibrations in the spanwise (β) and streamwise (α_{r}) wavenumber space was obtained.

7) The determination of the *resonant spectrum* of surface vibrations. To obtain this spectrum complex spectral amplitudes were determined for *resonant* wavenumbers $\tilde{\alpha}_{\mathrm{r}}(\beta)$. In a general case of interaction between the 2D acoustic wave and the surface vibrations the resonant wavenumbers for *plus combination mode* have to be determined as

$$\tilde{\alpha}_{\mathrm{r}+}(\beta) = \tilde{\alpha}_{\mathrm{rTS}+}(\beta) - \alpha_{\mathrm{rac}}, \tag{1}$$

and for *minus combination mode*

$$\tilde{\alpha}_{\mathrm{r}-}(\beta) = \alpha_{\mathrm{rac}} - \tilde{\alpha}_{\mathrm{rTS}-}(\beta), \tag{2}$$

where α_{rac} is the streamwise wavenumber of the acoustic wave, while $\tilde{\alpha}_{\mathrm{rTS}+} = \tilde{\alpha}_{\mathrm{rTS}+}(\beta)$ and $\tilde{\alpha}_{\mathrm{rTS}-} = \tilde{\alpha}_{\mathrm{rTS}-}(\beta)$ are the dispersion functions for the TS-modes excited at minus- and plus-regimes, respectively. The streamwise wavenumber α_{rac} is

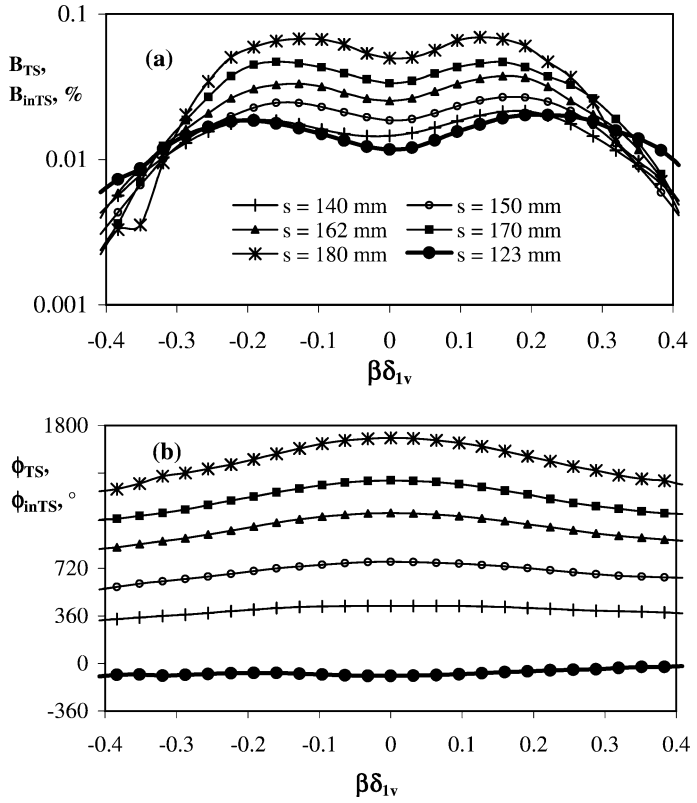

Fig. 10. Spatial evolution of amplitude (a) and phase (b) parts of the spanwise-wavenumber spectra of TS-waves excited at plus combination frequency $f_{TS2+} = f_{ac} + f_v = 1063$ Hz in regime $K = 0.217 f_{TS2+}$ and reconstructed initial spectra ($s_v = 123$ mm).

practically equal to zero because the acoustic wavelength involved is more than one order of magnitude greater than the TS-wavelengths. Also, the symmetry of the base flow provides the equality: $\tilde{\alpha}_{rTS+}(f_{TS}, \beta) = \tilde{\alpha}_{rTS-}(f_{TS}, \beta) = \tilde{\alpha}_{rTS}(f_{TS}, \beta)$. Due to these circumstances, the resonant wavenumbers were found during the data processing as:

$$\tilde{\alpha}_r(\beta) = \tilde{\alpha}_{rTS}(\beta). \tag{3}$$

The dispersion curves $\tilde{\alpha}_{rTS}(\beta)$ were determined for combination modes under investigation using the experimentally obtained streamwise phase distributions (like those shown in Fig. 10(b)).

8) The determination of the complex vibro-acoustic receptivity function, according to following definition (see e.g. [41]):

$$\overline{G}_{av}(f_{TS}, \beta) = G_{av}(f_{TS}, \beta)\, e^{i\phi_{av}(f_{TS},\beta)} = \frac{\overline{B}_{inTS}(f_{TS}, \beta)}{\overline{A}_{ac}(f_{ac})\widetilde{\overline{C}}_v(f_v, \tilde{\alpha}_r, \beta)}, \tag{4}$$

where

$$\overline{B}_{inTS}(f_{TS}, \beta) = B_{inTS}(f_{TS}, \beta)\, e^{i\phi_{inTS}(f_{TS},\beta)} \tag{5}$$

is the initial complex spectral amplitude of the TS-wave excited in the boundary layer and determined at step 5,

$$\overline{A}_{ac} = A_{ac}\, e^{i\phi_{ac}} \tag{6}$$

is the complex amplitude of the external acoustic perturbation measured in the free-stream at vibrator position,

$$\widetilde{\overline{C}}_v(f_v, \tilde{\alpha}_r, \beta) = \widetilde{\overline{C}}_v(f_v, \tilde{\alpha}_r, \beta)\, e^{i\phi_v(f_v,\tilde{\alpha}_r,\beta)} \tag{7}$$

is the complex resonant spectrum of the surface vibrations (determined at steps 6 and 7).

During the data processing all length scales were normalised by the boundary-layer displacement thickness $\delta_{1v} = 0.356$ mm at the location of the vibrator, while all velocities — by the boundary-layer-edge velocity $U_{ev} = 36.0$ m/s over the vibrator.

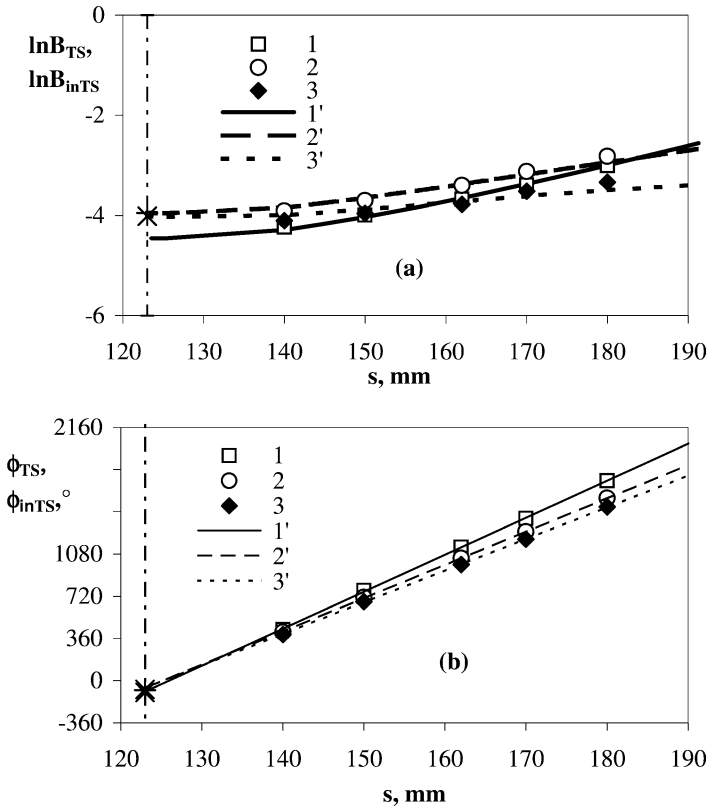

Fig. 11. Illustration of the procedure of reconstruction of initial spectral amplitudes (a) and phases (b) of TS-modes excited in the regime $K = 0.217 f_{TS2+}$ at plus combination frequency $f_{TS2+} = f_{ac} + f_v = 1063$ Hz for three fixed values of the spanwise wavenumber. Figure (a): points 1–3 – experimental TS spectral amplitudes for $\beta\delta_1 = 0,\ 0.192$, and 0.292. Lines 1′–3′ – corresponding approximations by LST. Figure (b): points 1–3 – experimental phases for $\beta\delta_1 = 0,\ 0.192$, and 0.292. Lines 1′–3′ – corresponding line approximations. Dash–dot line indicates the position of the vibrator, crosses – reconstructed initial amplitudes and phases.

5. Coefficients of vibro-acoustic receptivity and comparison with acoustic-roughness receptivity

The main results of study of the boundary-layer acoustic receptivity in presence of surface vibrations are presented in Figs. 12–15. The amplitudes (normalised by δ_{1v}) and phases of the complex receptivity coefficients are shown in Fig. 12 for regimes $K = 0.980 f_{TS2+}$, $K = 0.434 f_{TS2+}$, and $K = 0.217 f_{TS2+}$ (see Table 1), i.e. for three different values of parameter K but approximately the same TS-wave frequency ($F = 77.4 \times 10^{-6}$). The data are shown as functions of the non-dimensional spanwise wavenumber $\beta\delta_{1v}$, in a range between -0.3 to $+0.3$. For higher absolute values of $\beta\delta_{1v}$ the experimental accuracy was worse because these strongly inclined 3D waves (propagation angles are higher than 60 degrees), had typically very low amplitudes (see e.g. Fig. 10(a)). Similarly, Fig. 13 shows the receptivity data obtained in regimes $K = 0.217 f_{TS3+}$ and $K = 0.217 f_{TS4+}$, i.e. for fixed value of K and slightly different TS-wave frequencies ($F = 115.9 \times 10^{-6}$ and 120.3×10^{-6}, respectively).

It is seen from Fig. 12(a) that within an experimental accuracy the same receptivity coefficients are observed for all three values of parameter K in all three studied cases. In other words, the data obtained show that initial amplitudes of the TS-waves excited due to the interaction of acoustics and vibration *are independent of the parameter of non-stationarity K of the surface non-uniformity*. All investigated cases (Fig. 12(a) and Fig. 13(a)) demonstrate a higher efficiency of transformation of acoustic perturbations into 3D instability waves rather then into 2D ones. This property is stronger expressed for higher TS-wave frequencies (Fig. 13(a)). Indeed, for TS-wave frequency f_{TS2} (Fig. 12(a)) the receptivity amplitude observed for propagation angles about 50° ($\beta\delta_{1v} = 0.22$) is higher then that of the 2D-wave ($\beta\delta_{1v} = 0$) by a factor of *two* approximately. Meanwhile, for frequencies f_{TS3} and f_{TS4} (Fig. 13(a)), the receptivity amplitudes for 3D TS-waves with the same propagation angles ($\beta\delta_{1v} = 0.28$) is higher than that for the 2D-wave by a factor of *three*. At the same time, the receptivity for 2D waves depends

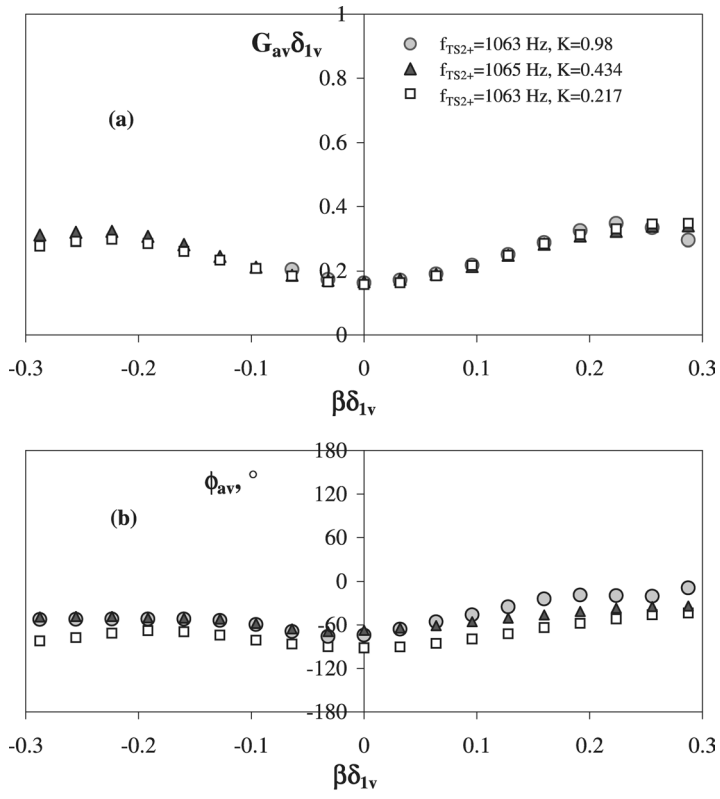

Fig. 12. Amplitudes (a) and phases (b) of vibro-acoustic receptivity coefficients versus spanwise wavenumber obtained for the frequency $f_{TS2} \approx 1063$ Hz in the regimes $K = 0.98 f_{TS2+}$, $K = 0.434 f_{TS2+}$, and $K = 0.217 f_{TS2+}$.

rather weakly on the TS-wave frequency. The phase parts of the receptivity functions (Fig. 12(b) and Fig. 13(b)) demonstrate relatively weak dependence on the spanwise wavenumber. Some visible differences in the receptivity phases are explained by a restricted accuracy of determination of the initial TS-wave phases (see Section 4). This point is especially clear seen from comparison of the results obtained for the same values of K and for very close values of the TS-wave frequency shown in Fig. 13(b).

As was mentioned above, frequencies f_{TS2} and f_{TS3} were chosen to be close to those investigated by Würz et al. [41] in the case of scattering of acoustic waves on *steady* surface roughness. In terms of the present investigation, the case studied in [41] can be considered as that with $f_v \approx 0$ and, hence, $K \approx 0$ (despite in the experimental part of that work K was equal to 0.016). The comparison of those data with the present results, obtained for $K \neq 0$, is shown in Fig. 14, where the receptivity coefficients for TS-wave frequency f_{TS2} are presented together with those obtained in [41] experimentally and numerically (DNS). A similar comparison for higher frequency f_{TS3} is presented in Fig. 15. (The differences between compared frequencies studied in the present work and in [41] are less than 2%.) The data shown in Figs. 14 and 15 are plotted versus the TS-wave propagation angle rather than versus the spanwise wavenumber as in Figs. 12 and 13. All results presented in Figs. 14 and 15 demonstrate a very well agreement of the receptivity functions, especially for small and moderate propagation angles, where the experimental accuracy is better. Similar to Fig. 12, this comparison supports the conclusion drawn above that the studied receptivity mechanism is independent of the parameter of non-stationarity of the surface non-uniformities K, in the range of studied parameters which starts from $K = 0.98$, when the vibration and acoustic frequencies (f_v and f_{ac}) are very close to each other, to the extreme case of stationary surface roughness with $K = 0$ ($f_v = 0$, $f_{TS} = f_{ac}$). Fig. 15 shows also that this independence is observed at higher TS-wave frequencies as well. Therefore: *the vibro-acoustic receptivity is independent of both the acoustic frequency and the vibration frequency and depends only on the frequency of the excited TS-waves*. This result means, in particular, that the *vibro-acoustic* receptivity coefficients can be estimated in the framework of *acoustic-roughness* receptivity theories.

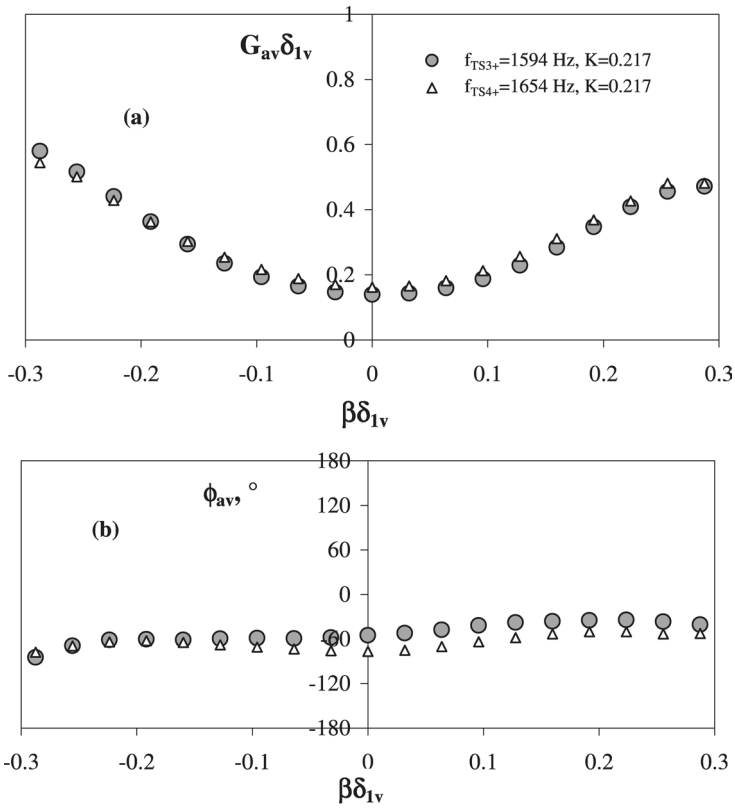

Fig. 13. Amplitudes (a) and phases (b) of vibro-acoustic receptivity coefficients versus spanwise wavenumber obtained for close frequencies $f_{TS3} = 1594$ Hz and $f_{TS4} = 1654$ Hz in the regimes $K = 0.217 f_{TS3+}$ and $K = 0.217 f_{TS4+}$.

6. Results of measurements in minus-regimes

6.1. Anomalous disturbance behaviour

A typical frequency spectrum of disturbances measured in the boundary layer at minus-regime $K = 0.217 f_{TS2-}$ is presented in Fig. 16. The general view of the spectrum is similar to that shown in Fig. 8 for plus-regime $K = 0.217 f_{TS2+}$. The strongest disturbances in the spectrum are also observed at acoustic frequency $f_{ac} = 1359$ Hz (marked with a triangle) and at vibration frequency $f_v = 295$ Hz (marked with a closed circle). The minus combination peak at $f_{TS2-} = f_{ac} - f_v = 1064$ Hz represents the frequency of interest here (which coincides, practically, with the frequency of the TS-wave excited in plus-regime $K = 0.217 f_{TS2+}$). Spatial development of disturbances excited at this frequency is shown in Fig. 17 as a set of spanwise distributions of the disturbance amplitudes (Fig. 17(a)) and phases (Fig. 17(b)) measured at several streamwise positions. It is easy to see, that the shape of the wave-train observed in minus-regime $K = 0.217 f_{TS2-}$ looks significantly different from that found in plus-regime $K = 0.217 f_{TS2+}$ (cf. Fig. 9). A deep spanwise modulation of the boundary-layer disturbances observed in the minus-regime suggests that some strongly inclined (essentially 3D) modes dominate in this case in the wave-train. This is actually observed in Fig. 18(a) where the amplitude parts of the corresponding spanwise-wavenumber spectra are presented. (The phase parts are shown in Fig. 18(b).) Moreover, the normalisation of the boundary-layer disturbance amplitudes by the amplitudes of the acoustic wave and the surface vibration have shown that these normalised amplitudes are much higher in minus-regime $K = 0.217 f_{TS2-}$ compared to those for plus-regime $K = 0.217 f_{TS2+}$. The results obtained in others minus-regimes ($K = 0.217 f_{TS3-}$ and $K = 0.434 f_{TS2-}$) display qualitatively similar but even stronger difference between the corresponding (to each other) pairs of minus- and plus-regimes.

Additional analysis of properties of the boundary-layer perturbations excited at the minus combination frequencies ($f_{TS-} = f_{ac} - f_v$) have shown that the amplification rates of these modes are very much different from (larger than, usually) those predicted by the linear stability theory, as well as those observed in the corresponding plus-regimes. This fact is illustrated in Fig. 19 where the spectral-mode amplification curves (symbols and thin lines) obtained in minus-regime $K = 0.217 f_{TS2-}$ are shown for three different values of the spanwise wavenumber in comparison with the curves calculated for 3D TS-modes (thick

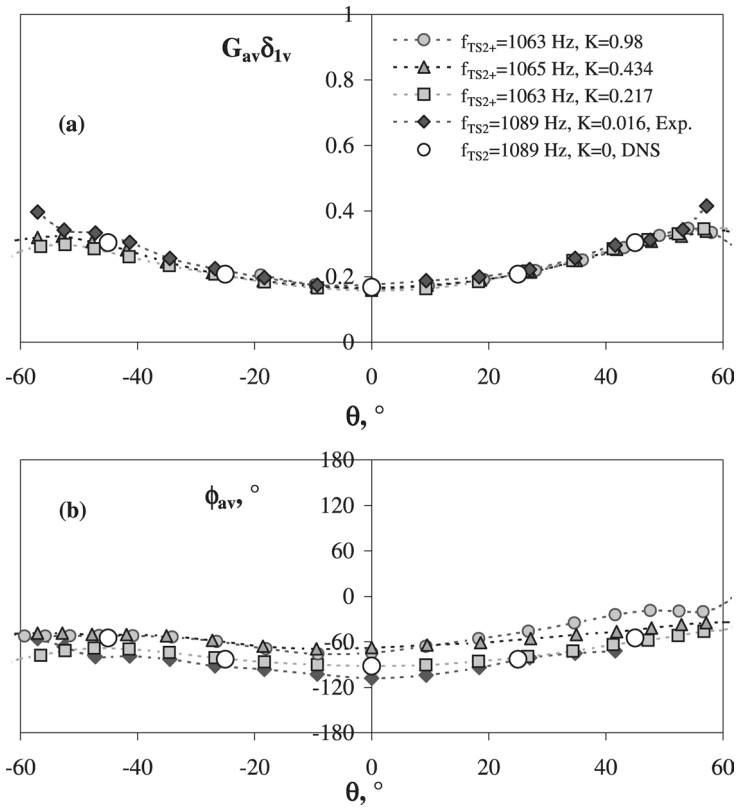

Fig. 14. Comparison of amplitudes (a) and phases (b) of vibro-acoustic receptivity coefficients for three different values of $K \neq 0$ with those obtained in [41] for $K \approx 0$ for the TS-wave frequency f_{TS2}.

lines). Note that in the corresponding plus-regime $K = 0.217 f_{TS2+}$ the amplification curves obtained for the same modes of the frequency-wavenumber spectrum (Fig. 11(a)) demonstrate a good agreement with the same calculated curves.

The unexpected phenomenon of the *anomalous behaviour* of the excited boundary-layer perturbations described above has been found also in all other studied *minus-regimes* but it has never been observed in any of studied *plus-regimes*.

6.2. Linearity of disturbance behaviour

The most natural explanation of the anomalous disturbance behaviour observed in minus-regimes is associated with a possible non-linearity of the problem under investigation. It has been assumed that the closeness of the minus combination modes to the frequency of subharmonic of the acoustic wave could lead to a subharmonic-type weakly-nonlinear interaction [46–50]. This interaction could occur between a quasi 2D TS-wave, excited at frequency f_{ac} by the acoustics on natural (two-dimensional mainly) non-uniformities of the base flow and the airfoil, and some of 3D TS-waves excited at frequencies f_v which then interact with $f_{TS-} = f_{ac} - f_v$. The former is excited directly by the vibrator, while the latter — by the vibro-acoustic receptivity mechanism under investigation. Note, that in this case $f_v = f_{ac}/2 - \Delta f$ and $f_{TS-} = f_{ac}/2 + \Delta f$, where $\Delta f = (f_{ac} - 2f_v)/2$, i.e. these frequency modes can be regarded as two quasi-subharmonic disturbances (with frequency detuning Δf) symmetric with respect to the subharmonic frequency $f_{ac}/2$. In order to check the applicability of this explanation, as well as the linearity of the studied receptivity problem, special measurements — non-linearity tests, were performed. The results obtained in one of such testes are presented below.

Namely, a measurement of a spanwise distribution was carried out inside the boundary layer at $s = 180$ mm in a regime, in which the disturbance frequencies were the same as in regime $K = 0.217 f_{TS3-}$ but the amplitudes of both the surface vibrations and the acoustic wave were intensified. In the main regime ($K = 0.217 f_{TS3-}$ itself) the r.m.s. amplitude A_v of the surface vibration was 29 μm in the vibrator center and the averaged intensity of velocity fluctuations A_{ac} in the acoustic field (over the vibrator center) was 0.0098 m/s (i.e. 0.272%). In the linearity test the measurement was performed when the amplitude of the surface vibrations was increased by a factor of 1.5 ($A_v = 44$ μm) and the acoustic perturbation was intensified by a factor of 1.4 ($A_{ac} = 0.0133$ m/s $= 0.37\%$). In case of a linear response of the boundary layer, such enhancement could

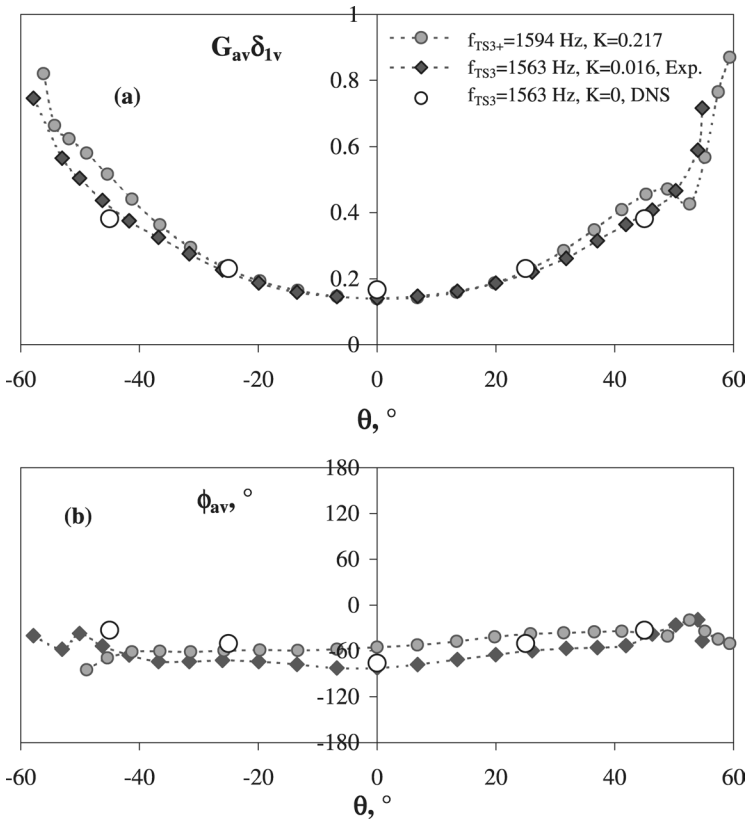

Fig. 15. Comparison of amplitudes (a) and phases (b) of vibro-acoustic receptivity coefficients for three different values of $K \neq 0$ with those obtained in [41] for $K \approx 0$ for the TS-wave frequency f_{TS3}.

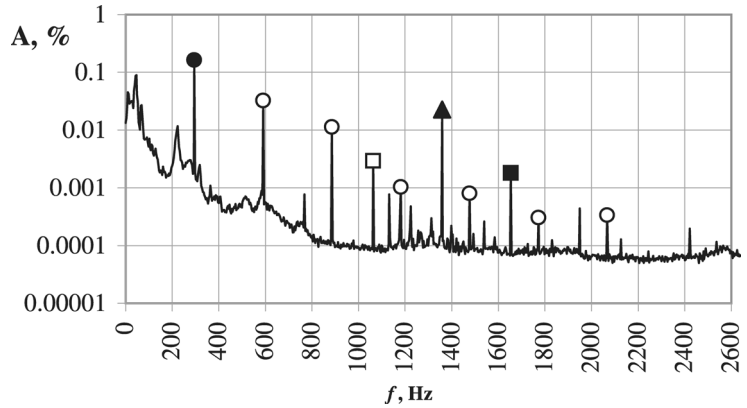

Fig. 16. Typical frequency spectrum of the hot-wire signal measured in the boundary layer in minus-regimes. Regime $K = 0.217 f_{TS2-}$, $s = 150$ mm. Closed circle: vibration frequency, open circles: harmonics of vibration frequency, closed triangle: acoustic frequency, closed square: plus combination mode, open square: minus combination mode.

result in an increase of the boundary-layer disturbance amplitude by a factor of $k_{lin} = 1.5 \times 1.4 = 2.1$. Meanwhile, it is known (see e.g. [48,49]) that the resonant-amplification increments of the subharmonic waves (as well as of frequency-detuned, i.e. quasi-subharmonic, ones) are nearly proportional to the fundamental-wave amplitude, i.e. to the acoustic amplitude in the present case. Therefore, in case of presence of the resonant amplification of the disturbances excited at the minus combination frequency we may expect a much larger increase of the boundary-layer disturbance amplitude.

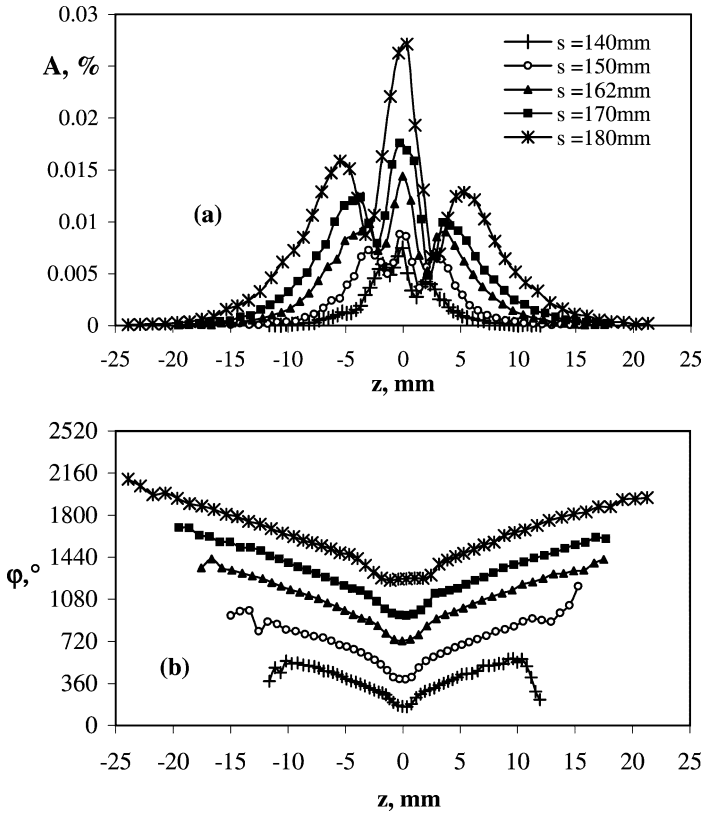

Fig. 17. Spatial development of amplitudes (a) and phases (b) of TS-waves excited at minus combination frequency $f_{TS2-} = f_{ac} - f_v = 1063$ Hz in the regime $K = 0.217 f_{TS2-}$.

Main result of the comparison of these two regimes is presented in Fig. 20 as two spanwise distributions of the disturbance amplitudes and phases measured at normal and enhanced amplitudes of the external perturbations. The amplitude distribution measured in the case of the enhanced perturbations is divided by factor $k_{lin} = 2.1$. A nearly perfect agreement of the two distributions (as well as similar agreement obtained in several other non-linearity tests) denotes undoubtedly the linearity of the two mechanisms: (i) the boundary-layer vibro-acoustic receptivity and (ii) the boundary-layer stability. This means that, first, all main receptivity results obtained in the present study at relatively low disturbance amplitudes (i.e. in the regimes listed in Table 1) correspond to the *linear receptivity problem* and, second, the *anomalous disturbance behaviour* observed in minus-regimes *cannot be explained by a nonlinearity*.

Attempts to find other explanation of this phenomenon, such as influence of an admixture of signals associated directly with acoustics or with probe vibrations, have not given any positive results. The only remaining explanation seemed to be connected with the presence of a distributed receptivity mechanism for scattering of acoustic waves (at f_{ac}) on a TS-wave-train excited by vibrations at frequency f_v. Such mechanism could lead both to a modification of the disturbance growth rates at combination frequencies and to a linear response of the boundary layer. In particular, such mechanism could result in a faster disturbance growth in cases when the streamwise-wavenumber resonant condition for the distributed excitation is satisfied (see e.g. [51]). However, the applicability of this explanation remains unclear. In particular, it is not clear why this mechanism has to work in all studied minus-regimes, despite the conditions of the streamwise-wavenumber resonance seem to be not satisfied in all cases, but does not work in all studied plus-regimes.

6.3. Estimates of relative receptivity amplitudes in minus-regimes

The anomalous disturbance behaviour has made it impossible to apply theoretical amplification curves for determination of initial instability wave amplitudes and, consequently, to determine quantitatively the receptivity coefficients in the minus-regimes. The attempts to obtain the initial disturbance amplitudes by means of upstream extrapolation of the data with the help of some arbitrary functions (similar to experiments [12,13]) do not give reliable results at the present experimental conditions. The problem is connected with a too complicated disturbance behaviour, which includes (in particular) some regions of attenuation

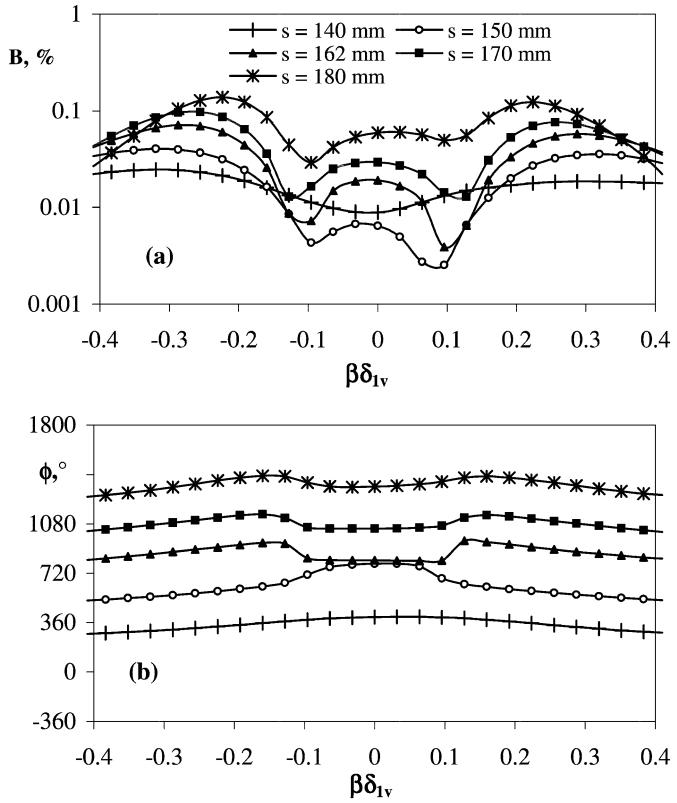

Fig. 18. Spatial development of amplitude (a) and phase (b) parts of spanwise-wavenumber spectra of TS-waves excited at minus combination frequency $f_{TS2-} = f_{ac} - f_v = 1063$ Hz in the regime $K = 0.217 f_{TS2-}$.

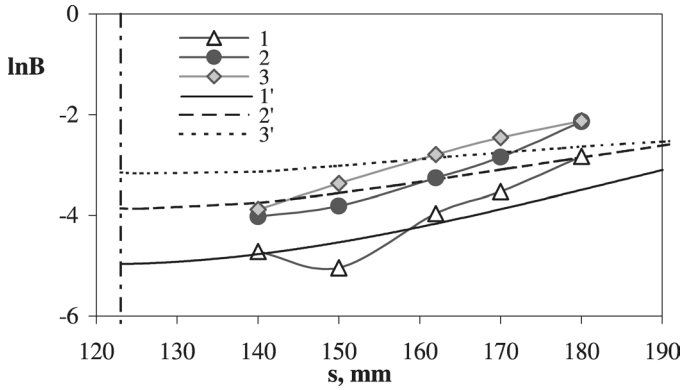

Fig. 19. Illustration of the anomalous behaviour of spectral amplitudes of boundary-layer disturbances excited in the minus-regime $K = 0.217 f_{TS2-}$ at minus combination frequency $f_{TS2-} = 1064$ Hz in comparison with linear stability theory for three fixed values of the spanwise wavenumber. Points 1–3 – experimental spectral amplitudes for $\beta\delta_1 = 0,\ 0.192$, and 0.292. Lines $1'$–$3'$ – corresponding amplitude distributions calculated with LST.

(see e.g. Fig. 19, $\beta = 0$). However, an attempt to make at least some rough estimates of initial TS-wave amplitudes has been made in order to evaluate relative values of the vibro-acoustic receptivity coefficients observed in minus-regimes in comparison with plus-regimes.

It tuned out that such estimates can be obtained integrally for the whole spanwise-wavenumber spectrum. Total (integral) amplitudes A_{int} of boundary-layer perturbations were determined in every streamwise location for the excited TS-wave train as a whole. These amplitudes were found by integration of amplitude spanwise distributions (like those shown in Fig. 9(a) and

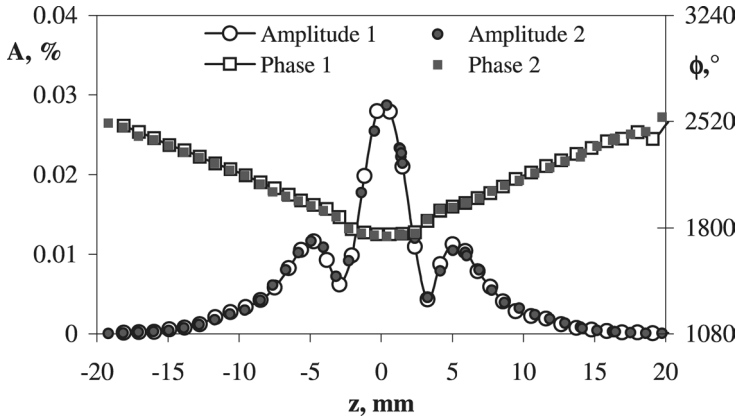

Fig. 20. Results of the linearity test. Spanwise distributions of boundary-layer disturbance amplitude and phase measured in the minus-regime $K = 0.217 f_{\mathrm{TS3}-}$ at normal excitation (1) and at enhanced excitation (2). Amplitudes measured at enhanced excitation are divided by a factor of $k_{\mathrm{lin}} = 2.1$.

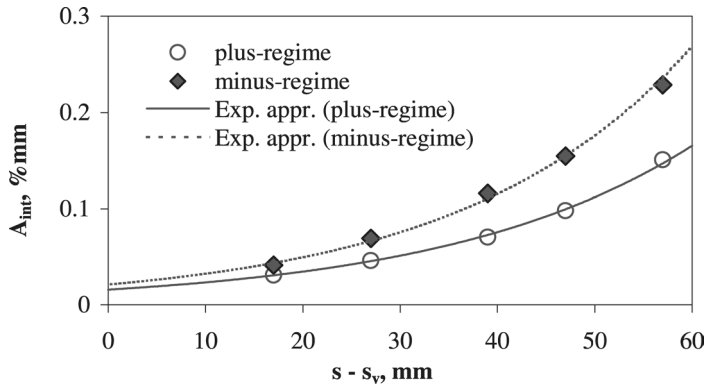

Fig. 21. Downstream growth of the integral intensity of TS-waves in the whole spanwise-wavenumber spectrum. Comparison of minus-regime $K = 0.217 f_{\mathrm{TS2}-}$ and plus-regime $K = 0.217 f_{\mathrm{TS2}+}$ for the TS-wave frequency $f_{\mathrm{TS2}} \approx 1063$ Hz. Points: experimental data, curves: their exponential approximation and extrapolation.

Fig. 17(a)) in the spanwise direction. The resulting integral amplification curves obtained in the minus-regime $K = 0.217 f_{\mathrm{TS2}-}$ and in the corresponding plus-regime $K = 0.217 f_{\mathrm{TS2}+}$ are presented in Fig. 21 versus the streamwise distance from the vibrator. For better comparability of these two distributions the amplitudes A_{int} measured in minus-regime $K = 0.217 f_{\mathrm{TS2}-}$ are renormalised to the same vibrational and acoustic amplitudes as those measured in the corresponding plus-regime $K = 0.217 f_{\mathrm{TS2}+}$. The experimental points shown in Fig. 21 are approximated by exponents (curves). It is seen, first, that the exponential approximation fits reasonably good the measured distributions. Second, similarly to most of the individual spectral modes (Fig. 19) the *integral* disturbance intensity also grows faster in the minus-regime than in the plus-regime. This difference is found to be even greater for frequency f_{TS3} when comparing the regimes $K = 0.217 f_{\mathrm{TS3}-}$ and $K = 0.217 f_{\mathrm{TS3}+}$ (not shown). Third, the amplification curves shown in Fig. 21 (as well as similar curves obtained in two other studied cases) indicate that the *initial* (i.e. at $s_{\mathrm{v}} = 123$ mm) TS-wave amplitudes, estimated by the exponential approximations, are rather close to each other in the two regimes. The observed small difference might be explained just by an error of such a rough estimation. This means that the integral vibro-acoustic receptivity is also *approximately the same* in every corresponding pair of minus- and plus-regimes. Of course, this conclusion is not very strict. However, it supports the previous conclusion (made in Section 5) regarding the absence of any dependence of the receptivity coefficients on the specific frequencies of the involved vibrations and acoustic waves, despite these frequencies are very much different in every pair of plus- and minus-regimes corresponding to the same frequency of the excited TS-wave (see Table 1).

7. Conclusions

A set of experiments devoted to the problem of transformation of 2D acoustic waves into 3D TS-waves due to the scattering of the former on essentially non-stationary, 3D surface non-uniformities (vibrations) is performed on a 2D airfoil. The experiments are carried out at controlled disturbance conditions for various combinations of frequencies of the involved acoustic wave (f_{ac}) and the surface vibration (f_v). Three values of the parameter of non-stationarity $K = f_v/f_{ac}$ of the surface non-uniformity are investigated. The generation of instability waves is considered in two general cases: (i) at *plus* combination frequencies $f_{TS+} = f_{ac} + f_v$ and (ii) at *minus* combination frequencies $f_{TS-} = f_{ac} - f_v$. In the plus-regimes the complex coefficients (amplitude and phase) of the vibro-acoustic receptivity are obtained as functions of the spanwise wavenumber and the TS-wave propagation angle for three different values of the parameter K, as well as for different frequencies of the excited instability waves when the parameter K is fixed. In the minus-regimes some estimates of relative values of integral (in the spanwise-wavenumber spectrum) receptivity amplitudes are obtained in comparison with the corresponding plus-regimes (i.e. for the same values of parameter K and TS-wave frequency f_{TS}). These integral receptivity coefficients are found to be very close to each other in minus- and plus-regimes. Variation of the acoustic and vibration amplitudes have shown that the studied vibro-acoustic receptivity mechanism is linear in a sense that the receptivity amplitudes and phases are independent of the amplitudes of the involved external disturbances.

The main conclusion of the study is the following. For every studied value of the TS-wave propagation angle *the vibro-acoustic receptivity coefficients are independent of both the parameter of non-stationarity K of the surface non-uniformity and the specific frequencies of vibrations and acoustics. They depend only on the frequency of the excited TS-wave.* The comparison of the *vibro-acoustic receptivity* characteristics obtained in the present experiments with the *acoustic-roughness receptivity*, i.e. with the case of practically stationary surface non-uniformity, studied in [41] ($f_v \approx 0$, $K \approx 0$, $f_{TS} \approx f_{ac}$) has shown the same receptivity amplitudes and phases for all investigated TS-wave frequencies and spanwise wavenumbers. Thus, the conclusion formulated above is found to be valid in the range $0 \leqslant K \leqslant 0.98$. This means, in particular, that the vibro-acoustic receptivity coefficients can be estimated correctly on bases of acoustic-roughness receptivity theories. Note that despite the vibro-acoustic receptivity turned out to be very similar to the acoustic-roughness one, the former can play a very important role in the laminar-turbulent transition process because it provides a redistribution of the disturbance energy in the frequency-wavenumber spectrum. Due to this redistribution, the vibro-acoustic receptivity can lead to excitation of strongly amplified TS-waves even in cases when the instability waves excited directly by both the acoustic wave and the surface vibrations are far from the instability region.

Common properties of the studied acoustic receptivity mechanism (due to either surface vibration or surface roughness) are the following. The excitation of *three-dimensional* TS-waves due to scattering of 2D acoustics on 3D surface vibrations is significantly more efficient than the corresponding excitation of two-dimensional TS-waves. For all TS-wave propagation angles the acoustic receptivity amplitudes increase with the TS-wave frequency. However, this frequency dependence is very weak for excitation of 2D instability waves and increases quickly with the TS-wave propagation angle. The acoustic receptivity phases are found to depend rather weakly on the wave inclination angle for all studied frequencies and parameters K.

An anomalous behaviour of the TS-waves excited by the vibro-acoustic receptivity mechanism in minus-regimes was found in the present study. The amplification of these modes differs from that observed in the corresponding plus-regimes and predicted by the linear stability theory. The strongest amplification in the minus-regimes is found for essentially 3D modes. It is shown that the phenomenon of the anomalous TS-wave behaviour in the minus-regimes *cannot* be explained by non-linearity of the associated stability or receptivity problem. The causes of this phenomenon remain unclear and need additional investigation.

Being obtained in Fourier space the linear coefficients of the vibro-acoustic receptivity are independent of the specific shape (and the frequency-wavenumber spectrum) of the surface vibrator, as well as of the specific frequency spectrum of the acoustic wave. These results can be directly used for estimates of initial amplitudes of the excited 3D TS-waves, as well as for validations of theoretical and numerical approaches.

Acknowledgements

This work is supported by grants of the German Research Foundation (DFG) and is a part of the research program ‘Transition’.

References

[1] M.V. Morkovin, Critical evaluation of transition from laminar to turbulent shear layer with emphasis of hypersonically traveling bodies, AFFDL Tech. Rep. 68–149, 1968.

[2] Y.S. Kachanov, V.V. Kozlov, V.Y. Levchenko, Beginning of Turbulence in Boundary Layer, Nauka, Siberian Div., Novosibirsk, 1982 (in Russian).
[3] Y.S. Kachanov, Three-dimensional receptivity of boundary layers, Eur. J. Mech. B Fluids 19 (5) (2000) 723–744.
[4] M. Gaster, On the generation of spatially growing waves in a boundary layer, J. Fluid Mech. 22 (1965) 433–441.
[5] E.D. Terent'ev, A linear problem on a vibrator in subsonic boundary layer, Prikl. Mat. Mekh. 45 (6) (1981) 1049–1055 (in Russian).
[6] A.M. Tumin, A.V. Fyodorov, Generation of instability waves in a boundary layer on a vibrating surface, Zh. Prikl. Mekh. Tekh. Fiz. 3 (1983) 72–79 (in Russian).
[7] A.M. Tumin, A.V. Fyodorov, Generation of instability waves in boundary layer by localized vibrator, Zh. Prikl. Mekh. Tekh. Fiz. 6 (1984) 65–72 (in Russian).
[8] V.M. Gilyov, V.V. Kozlov, Excitation of Tollmien–Schlichting waves in a boundary layer on a vibrating surface, Zh. Prikl. Mekh. Tekh. Fiz. 6 (1984) 73–77 (in Russian).
[9] E.D. Terent'ev, A linear problem on a vibrator oscillating harmonically at supercritical frequencies in a subsonic boundary layer, Prikl. Mat. Mekh. 48 (2) (1984) 264–272 (in Russian).
[10] A.V. Fyodorov, Generation of Tollmien–Schlichting waves in a boundary layer by means of a periodic external perturbation localized on the surface, Izv. Akad. Nauk SSSR Mekh. Zhidk. i Gaza 6 (1984) 36–41 (in Russian).
[11] A.V. Fyodorov, Excitation of cross-flow instability waves in boundary layer on a swept-wing, Zh. Prikl. Mekh. Tekhn. Fiz. 5 (1988) 46–52 (in Russian).
[12] A.V. Ivanov, Y.S. Kachanov, T.G. Obolentseva, A. Michalke, Receptivity of the Blasius boundary layer to surface vibrations. Comparison of theory and experiment, in: 9th Int. Conference on Methods of Aerophysical Research. Proceedings. Part I, Inst. Theor. & Appl. Mech., Novosibirsk, 1998, pp. 93–98.
[13] V.R. Gaponenko, A.V. Ivanov, Y.S. Kachanov, J.D. Crouch, Swept-wing boundary-layer receptivity to surface non-uniformities, J. Fluid Mech. 461 (2002) 93–126.
[14] S. Bake, A.V. Ivanov, H.H. Fernholz, K. Neemann, Y.S. Kachanov, Receptivity of boundary layers to three-dimensional disturbances, Eur. J. Mech. B Fluids 21 (1) (2002) 29–48.
[15] Y.S. Kachanov, D.B. Koptsev, B.V. Smorodsky, Study of three-dimensional receptivity of a 2D boundary layer with a positive pressure gradient to surface vibrations. Experiment and theory, Thermophys. Aeromech. 9 (3) (2002) 371–392.
[16] V.N. Zhigulyov, A.M. Tumin, Origin of Turbulence, Nauka, Novosibirsk, 1987 (in Russian).
[17] M.E. Goldstein, L.S. Hultgren, Boundary-layer receptivity to long-wave free-stream disturbances, Ann. Rev. Fluid Mech. 21 (1989) 137–166.
[18] E.J. Kerschen, Boundary layer receptivity, AIAA Pap. No. 89-1109, 1989.
[19] V.V. Kozlov, O.S. Ryzhov, Receptivity of boundary layers: asymptotic theory and experiment, Proc. Roy. Soc. London Ser. A 429 (1990) 341–373.
[20] M.V. Morkovin, E. Reshotko, Dialogue on progress and issues in stability and transition research, in: D. Arnal, R. Michel (Eds.), Laminar-Turbulent Transition, Springer, Berlin, 1990, pp. 3–29.
[21] M. Choudhari, C.L. Streett, A finite Reynolds number approach for the prediction of boundary-layer receptivity in localized regions, Phys. Fluids A 4 (1992) 2495–2514.
[22] J.D. Crouch, Theoretical studies on the receptivity of boundary layers, AIAA Pap. No. 94-2224, 1994.
[23] M. Choudhari, Roughness-induced generation of crossflow vortices in three-dimensional boundary layers, Theoret. Comput. Fluid Dynamics 6 (1) (1994) 1–30.
[24] L.B. Aizin, N.F. Polyakov, Acoustic generation of Tollmien–Schlichting waves over local unevenness of surfaces immersed in streams, Preprint No. 17, Inst. Theor. & Appl. Mech., Novosibirsk, 1979 (in Russian).
[25] V.S. Kosorygin, V.Y. Levchenko, N.F. Polyakov, On generation and evolution of waves in laminar boundary layer, in: V.V. Kozlov (Ed.), Laminar-Turbulent Transition, Springer, Berlin, 1985, pp. 233–242.
[26] V.S. Kosorygin, Experimental investigation of flat plate laminar boundary layer under low natural and acoustic disturbances, PhD Thesis, Inst. Theor. & Appl. Mech., Novosibirsk, 1986 (in Russian).
[27] W.S. Saric, J.A. Hoos, Y. Kohama, Boundary-layer receptivity: part 1: Freestream sound and 2D roughness strips, Report, CEAS-CR-R-90191, Arizona State University, College of Engineering and Applied Sciences, Tempe, 1990.
[28] M. Wiegel, R.W. Wlezien, Acoustic receptivity of laminar boundary layers over wave walls, AIAA Paper 93-3280, 1993.
[29] V.S. Kosorygin, R.H. Radeztsky. Jr., W.S. Saric, Laminar boundary layer sound receptivity and control, in: R. Kobayashi (Ed.), Laminar-Turbulent Transition, Springer, Berlin, 1995, pp. 517–524.
[30] M. Choudhari, E.J. Kerschen, Instability wave patterns generated by interaction of sound wave with three-dimensional wall suction or roughness, AIAA Paper 90-0119, 1990.
[31] M. Tadjfar, R.J. Bodonyi, Receptivity of laminar boundary layer to the interaction of a three dimensional roughness element with time-harmonic free-stream disturbances, J. Fluid Mech. 242 (1992) 701–720.
[32] M. Tadjfar, Receptivity of laminar boundary layer to the interaction of a three dimensional roughness element with time-harmonic free-stream disturbances, PhD thesis, Dept. Aero. & Astro. Engrg., Ohio State University, 1990.
[33] M.D. Zhou, D.P. Liu, R.F. Blackwelder, An experimental study of receptivity of acoustic waves in laminar boundary layers, Exp. Fluids 17 (1994) 1–9.
[34] L.M. Cullen, H.P. Horton, Acoustic receptivity in boundary layers with surface roughness, in: H. Fasel, W. Saric (Eds.), Laminar-Turbulent Transition, Springer, Berlin, 2000, pp. 43–50.
[35] J.D. Crouch, Receptivity of three-dimensional boundary layers, AIAA Paper 93-0074, 1993.

[36] A.V. Ivanov, Y.S. Kachanov, D.B. Koptsev, Method of phased roughness for determining the acoustic receptivity coefficients, in: 9th Int. Conference on Methods of Aerophysical Research. Proceedings. Part II, Inst. Theor. & Appl. Mech., Novosibirsk, 1998, pp. 89–94.
[37] A.V. Ivanov, Y.S. Kachanov, D.B. Koptsev, Excitation of cross-flow instability waves by acoustic field in presence of a surface roughness, Thermophys. Aeromech. 8 (3) (2001) 371–389.
[38] A.V. Ivanov, Y.S. Kachanov, D.B. Koptsev, An experimental investigation of instability wave excitation in three-dimensional boundary layer at acoustic wave scattering on a vibrator, Thermophys. Aeromech. 4 (4) (1997) 359–372.
[39] W. Würz, S. Herr, S. Wagner, Y.S. Kachanov, Experimental investigation on three-dimensional acoustic receptivity of a laminar boundary layer in the presence of surface non-uniformities, in: W. Nitsche, H.J. Heinemann, H. Hilbig (Eds.), New Results in Numerical and Experimental Fluid Mechanics. 11.DGLR/AG-STAB Fach-Symposium, Berlin 10-12.11.1998, NNFM, vol. 72, Vielweg, Wiesbaden, 1998, pp. 529–536.
[40] W. Würz, S. Herr, A. Wörner, U. Rist, S. Wagner, Y.S. Kachanov, Study of 3D wall roughness acoustic receptivity on an airfoil, in: H. Fasel, W. Saric (Eds.), Laminar-Turbulent Transition, Springer, Berlin, 2000, pp. 91–96.
[41] W. Würz, S. Herr, A. Wörner, U. Rist, S. Wagner, Y.S. Kachanov, Three-dimensional acoustic-roughness receptivity of a boundary layer on an airfoil: experiment and direct numerical simulations, J. Fluid Mech. 478 (2003) 135–163.
[42] W. Würz, Hitzdrahtmessungen zum laminar-turbulenten Strömungsumschlag in anliegenden Grenzschichten und Ablöseblasen sowie Vergleich mit der linearen Stabilitätstheorie und empirischen Umschlagskriterien, Dissertation, Institut für Aero- und Gasdynamik der Universität Stuttgart, 1995.
[43] M. Drela, M.B. Giles, Viscous-inviscid analysis of transonic and low Reynolds number airfoils, AIAA-86-1786-CP, 1986.
[44] T. Cebeci, A.M.O. Smith, Analysis of Turbulent Boundary Layers, Academic Press, New York, 1974.
[45] S.D. Conte, The numerical solution of linear boundary value problems, SIAM Rev. 8 (1966) N 3.
[46] Y.S. Kachanov, V.Y. Levchenko, The resonant interaction of disturbances at laminar-turbulent transition in a boundary layer, Preprint No. 10-82, 1982 (in Russian), Novosibirsk. Inst. Theor. & Appl. Mech., Siberian Div. USSR Acad. Sci.;
See also: Y.S. Kachanov, V.Y. Levchenko, J. Fluid Mech. 138 (1984) 209–247.
[47] T.C. Corke, R.A. Mangano, Resonant growth of three-dimensional modes in transitioning Blasius boundary layers, J. Fluid Mech. 209 (1989) 93–150.
[48] V.I. Borodulin, Y.S. Kachanov, D.B. Koptsev, Experimental study of resonant interactions of instability waves in self-similar boundary layer with an adverse pressure gradient: I. Tuned resonances, J. Turbulence 3 (2002) 062, 38.
[49] V.I. Borodulin, Y.S. Kachanov, D.B. Koptsev, A.P. Roschektayev, Experimental study of resonant interactions of instability waves in self-similar boundary layer with an adverse pressure gradient: II. Detuned resonances, J. Turbulence 3 (2002) 063, 22.
[50] V.I. Borodulin, Y.S. Kachanov, D.B. Koptsev, Experimental study of resonant interactions of instability waves in self-similar boundary layer with an adverse pressure gradient: III. Broadband disturbances, J. Turbulence 3 (2002) 064, 19.
[51] V.I. Borodulin, A.V. Ivanov, Y.S. Kachanov, A.A. Fedenkova, Distributed boundary-layer receptivity to non-stationary vortex disturbances with wall-normal vorticity in presence of surface non-uniformities, Thermophys. Aeromech., 2003, in press.